THE ASTROPHYSICAL JOURNAL, 451:156–166, 1995 September 20

THE CENTRAL REGIONS OF NGC 4691: A REMARKABLE STRUCTURE WITH A FAST OUTFLOW NEAR THE NUCLEUS

J. A. GARCÍA-BARRETO,[1] J. FRANCO,[1] J. GUICHARD,[2] AND R. CARRILLO[1]
Received 1995 January 5; accepted 1995 March 31

ABSTRACT

We present new R, I, and Hα imaging, and spectroscopy near Hα, for the barred galaxy NGC 4691. A remarkable structure in the innermost regions, composed of four main unresolved sources symmetrically distributed around the center, is apparent in all R, I, and Hα images. The spectroscopic data reveal the existence of a broad Hα component, $\Delta V_{\rm FWHM} \simeq 1207^{+180}_{-5}$ km s^{-1}, with a centroid that is blueshifted by some 500 km s^{-1} with respect to the normal emission of the galaxy. We interpret this broad-line component as an outflow that is pushing gas out of the plane of the galaxy, most probably due to compact supernova remnants inside dense H II circumnuclear regions.

Subject headings: galaxies: individual (NGC 4691) — galaxies: jets — galaxies: nuclei — infrared: galaxies

1. INTRODUCTION

Strong galactic outflows and winds have been observed in bright far-infrared galaxies including M82 (Bland & Tully 1988), NGC 253 (Ulrich 1978), NGC 3079 (Filippenko & Sargent 1992; Duric & Seaquist 1988), NGC 4945 (Whiteoak & Gardner 1979), Arp 220, and NGC 6240 (Heckman, Armus, & Miley 1987). In all cases, broad optical lines from the nuclear region are interpreted as gas being blown out of the disk into the halo by the action of a "superwind." Here we present optical spectroscopic evidence that suggests the existence of a fast outflow in the barred spiral galaxy NGC 4691. This outflow, an ionized shell expanding with velocities of about $V \sim 500$ km s^{-1} and blowing gas out of the plane of the galaxy, is probably a result of the action of compact SN remnants expanding inside H II regions near the nucleus.

NGC 4691 has been classified as an SBb pec and as an RSBS0P (i.e., outer ring barred spiral early-type peculiar) in the RSA (Sandage & Tammann 1987) and the RC3 catalogs, respectively. In addition, it has been identified as an H II galaxy with a low ionization nucleus by Keel (1983). Long-exposure photographs of this galaxy, like those in Sandage (1962), indicate that it is almost face-on with a pair of spiral arms delineating a circle around the center with a P.A. of $\simeq 10°$. A stellar bar is also apparent with a P.A. $\simeq 90°$. The angular sizes of the optical disk and bar are 2.'8 × 2.'3 and 1.'0 × 0.'45, respectively. The heliocentric velocities for various lines are: $V_{\rm H\alpha} \simeq 1125$ km s^{-1} (Sandage 1978), $V_{\rm CO} = 1126$ km s^{-1} (Wiklind, Henkel, & Sage 1993), and $V_{\rm H\,I} = 1119$ km s^{-1} (Richter & Huchtmeier 1987). Here we adopt a distance of $D = 22.3$ Mpc ($H_0 = 75$ km s^{-1} Mpc^{-1}; Tully 1988), and therefore the linear scale would be $1'' \simeq 110$ pc.

Nuclear 10 μm emission has been reported by Devereux (1987), and the *IRAS* fluxes at the far-infrared bands suggest a dust temperature of 40 K. This is about 20% higher than the characteristic dust temperature of other isolated and barred galaxies, $\langle T_{\rm dust}\rangle \simeq 34$ K (Solomon & Sage 1988; García-Barreto et al. 1993), and it is comparable to the temperatures found in interacting galaxies, $\langle T_{\rm dust}\rangle \simeq 41$ K (Solomon & Sage 1988). Radio continuum observations at different wavelengths yield a spectral index $\alpha_6^{20} \simeq 0.46$ (García-Barreto et al. 1993), suggesting a strong contribution from thermal emission, most likely resulting from a recent episode of vigorous OB star formation. Atomic and molecular hydrogen observations indicate a ratio $S(1)/{\rm Br}\gamma \simeq 0.86$ (Puxley, Hawarden, & Mountain 1990), also suggesting the existence of a rich cluster of OB stars embedded in dense molecular clouds and providing a strong UV radiation field.

In this paper, we present new optical observations (imaging and spectroscopy) of the central regions of the galaxy. In § 2 we describe the equipment, procedures, and results of the optical observations. It contains a description of the spatial structure seen in the R, I, and Hα images, along with the spectroscopic results. The R, I, and Hα images reveal the existence of a complex inner structure with four maxima (knots), distributed in two symmetrical pairs around the center. Their spectra show the presence of "normal" H II region emission in all four knots, but the brightest one, in the western part of the inner structure, has an additional broad Hα component that is blueshifted with respect to the normal emission. Of particular importance for the discussion of the present data is the position of the nucleus. We describe the position of the nucleus adopted by different authors and give arguments based on our observations to identify the position of the nucleus in § 3 together with a discussion of the possible origins for the structure and the broad-line component. A brief description of models for expanding shells and galactic winds is presented in § 4, and the final conclusions are summarized in § 5.

2. OPTICAL OBSERVATIONS AND RESULTS

The optical observations were performed at the Observatorio Astronómico Nacional in San Pedro Mártir, Baja California, México, using the 2.12 m telescope f/7.5 equipped with a 1024 × 1024 Thompson CCD detector using the broadband Johnson filters R and I, and a set of narrow-band filters centered at the wavelength of Hα for imaging. For spectroscopy we used the same system coupled to a Boller & Chivens spectrograph. The detector scale gives a spatial resolution of 0.''25 per pixel in the imaging mode, giving a field of view of 4.'25 × 4.'25, and a 1.6 Å pixel^{-1} spectral resolution and a spatial resolution of 0.''73 pixel^{-1} in the spectroscopic mode. The details of the observing runs are summarized in Table 1.

[1] Instituto de Astronomía, Universidad Nacional Autónoma de México, Apdo. Postal 70-264, México D.F. 04510, México.
[2] Instituto Nacional de Astrofísica, Optica y Electrónica, Apdo. Postal 216, Puebla 72000, Pue., México.

TABLE 1

LOG OF OBSERVATIONS OF THE BARRED GALAXY NGC 4691

Observation Type	Date	Instrument	Filter
Imaging	1992 Jun 3	CCD 1024 × 1024	*R*, *I*, Hα
	1993 Dec 15	CCD 1024 × 1024	Hα
Spectroscopic.....	1993 May 31	B&C, CCD 1024	

Every image was bias-subtracted and then flat-fielded with the NOAO-IRAF software by using an average of three 5 s exposures of blank fields taken at twilight or sunrise. Different flats were obtained for each filter. Two images were taken with the broadband *R* ($\lambda_c \simeq 6340$ Å, $\Delta\lambda \simeq 400$ Å) and *I* ($\lambda_c \simeq 8040$ Å, $\Delta\lambda \simeq 1660$ Å) filters, each with 90 s. Two images, 300 s each, were taken with the narrow-band filters centered at $\lambda \simeq 6459$ Å with $\Delta\lambda \simeq 101$ Å, for the continuum, and at $\lambda \simeq 6607$ Å with $\Delta\lambda \simeq 89$ Å for the redshifted Hα plus continuum. All images were calibrated and edited for cosmic rays and bad pixels. A second set of narrow-band Hα images was obtained during 1993 December, in order to corroborate the structure seen in the first run in 1992 June. The new images were also bias-subtracted, flat-fielded, and calibrated using the same software. The final Hα images presented here were obtained by subtracting the continuum. In order to do this, we selected one pair of the 1992 June line + continuum and continuum images each of 300 s integration time observed one after the other with similar sky conditions. The image scale was 1:1 for the subtraction. The subtraction was done after the positions of field stars from both images were determined. After the subtraction, the field stars disappeared almost completely from the final Hα emission image. The seeing in 1992 June was about 1″–1.″3 with clear sky. No image has been amplitude calibrated. In both runs, 1992 June and 1993 December, the same Hα structures were observed, even though we had poorer sky conditions in 1993 December. For the *R* and *I* images, we selected the best single image in every filter; that is, we did not combine or add any pair of images. Figures 1*a* and 1*b* show the corresponding *R* and *I* images of NGC 4691, while Figure 2 shows the continuum-free Hα image.

The spectroscopic observations were done on 1993 May 31 with a Cassegrain spectrograph with 600 grooves mm^{-1} at a grating angle of 13°. The central wavelength was chosen in the red part of the spectrum in order to include the [N II], Hα, and [S II] lines. The scale was 0.″73 $pixel^{-1}$ and 1.6 Å $pixel^{-1}$ in the spatial and dispersion directions, respectively. The slit length was 80 pixels long by 10 pixels wide positioned at P.A. ≃ 90°, that is, E-W. The slit was positioned on the brightest optical region of the galaxy on the declination corresponding to the brightest two southern knots, later identified in this paper as knots 1 and 2. The on source time was 1200 s followed by a 1 s exposure of a tungsten lamp. The appropriate flats were used to flatten the galaxy spectra. The data were bias-subtracted and flat-fielded using the NOAO IRAF software. In order to extract the spectrum of the line emission from NGC 4691, we used the routine "apall" from IRAF, where we co-added the pixels involved in the galaxy spectra after defining the most adequate aperture. The "splot" subroutine was used to measure the strengths, central wavelengths, widths, and fluxes of the emission lines. Figure 3 (Plate 1) shows a gray-scale image of the spectra from the central region of the galaxy. The orientation is as follows: east is to the left, west is to the right, and the dispersion axis runs with λ increasing upward. Notice also that there are two spectra separated by 17 pixels. The eastern spectrum displays lines with similar properties at those reported in previous observations, but the western spectrum

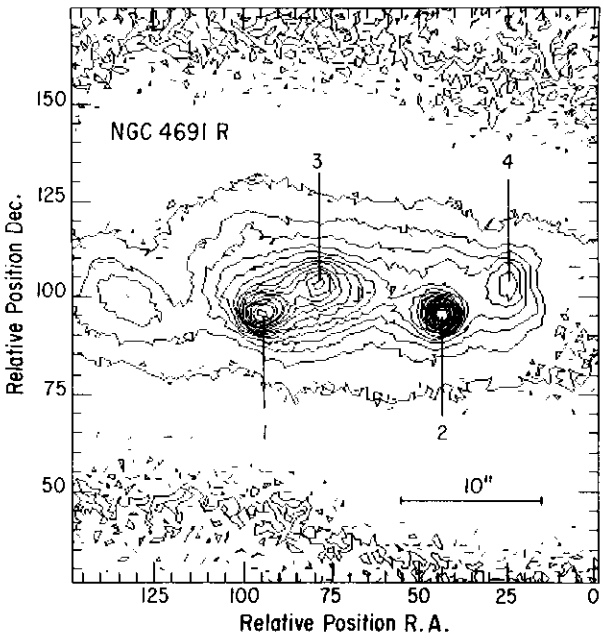

FIG. 1*a*

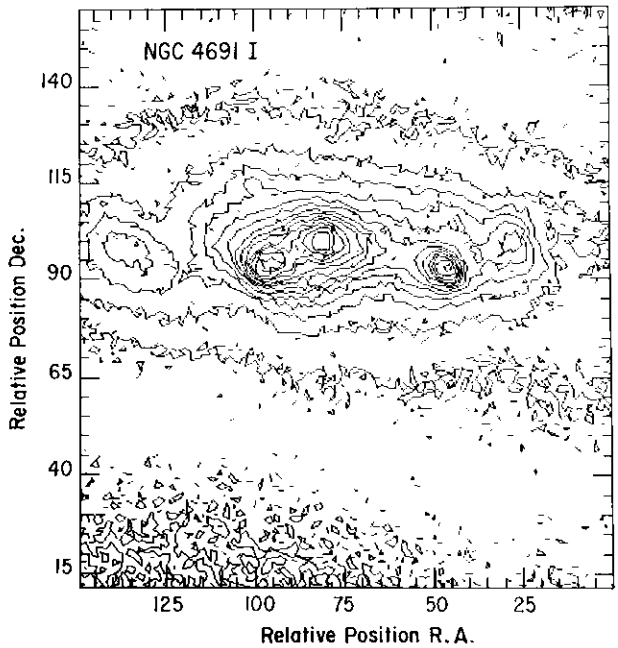

FIG. 1*b*

FIG. 1.—(*a*) Image of NGC 4691 in the broadband filter *R* ($\lambda_{central} \simeq 6340$ Å). The bar shows the angular scale for 10″; 1″ corresponds to a linear scale of 110 pc at a distance of 22.3 Mpc. Figures have not been amplitude calibrated. The four most intense peaks of the central structure are marked. North is up, east is left. (*b*) Image in the broadband filter *I* ($\lambda_{central} \simeq 8040$ Å). Scale and orientation are the same as in (*a*). Notice that similar structure is observed at *I* and *R* images, with knot 3 being the strongest at *I*.

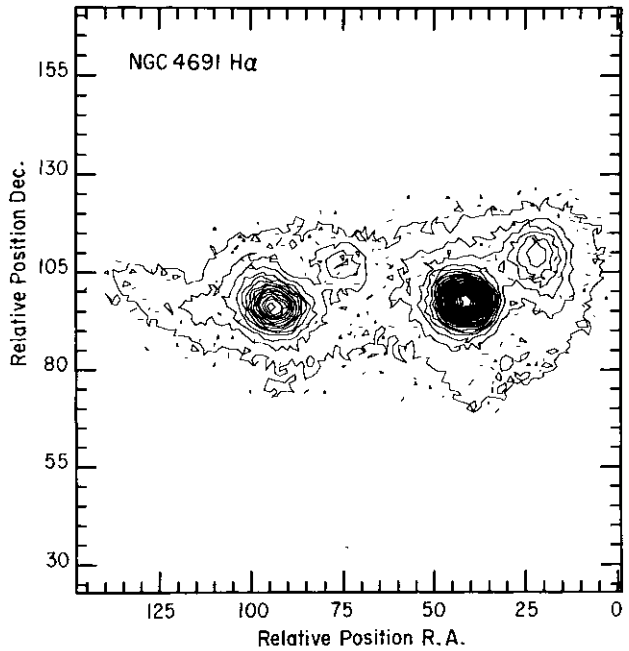

FIG. 2.—Images of NGC 4691 in the narrow-band filter Hα + N II after subtraction of the continuum. The four strong peaks are observed in this image, as they were in *R* and *I* images. In Hα, however, knot 3 is the weakest. Scale and orientation are the same as in Fig. 1.

has not been reported before (de Vaucouleurs & de Vaucouleurs 1967; Chromey 1974; Sandage 1978).

2.1. *The Spatial Structure of the Innermost Region*

Figures 1 and 2 show images in the *R*, *I*, and Hα filters of the innermost 38″ region of the barred galaxy NGC 4691. The same basic structure with four bright knots is present in all three images. It is difficult to distinguish which one of them, if any, is the compact nucleus of the galaxy, since there is no obvious dominant red peak. By analogy with other barred galaxies, like NGC 3351 where the compact nucleus is the strongest peak in the *I*-band image (Kennicutt, Keel, & Blaha 1989), the compact nucleus in NGC 4691 could be feature 3 in Figure 1*a*. The two main arguments in favor of this are that (a) it is the strongest feature in the *I*-band image, and (b) it is much weaker in the Hα image. Nonetheless, this is only a possibility, and more observations and dynamical studies are needed to determine the exact position of the compact nucleus. Figure 4*a* shows slices of the *I*, *R*, and Hα images taken across the galaxy to the E-W direction at the declination of the two bright knots labeled 3 and 4 in Figure 1*a*. Figure 4*b* shows the corresponding slices of the *I*, *R*, and Hα images taken at the declination of knots 1 and 2.

The relative separation and strengths of each bright knot in the three images is listed in Table 2. Notice that the relative séparation of knots 1 and 2 is about 12″.5, similar to the separation of ∼13″.3 between knots 3 and 4. Similarly, the separation in declination between knots 1 and 3, some 4″, is similar to the separation between knots 2 and 4, which is about 4″.7. The FWHM diameter for knot 1, about 2″.2, is very similar to that of knot 2 in all three images. This indicates that the knots are barely resolved and that their angular extent corresponds to about 240 pc in linear diameter. The same occurs with the FWHM diameters of knots 3 and 4, which are about 2″ in the three images.

TABLE 2

RELATIVE POSITIONS AND STRENGTHS OF THE STRONGEST PEAKS IN NGC 4691

Image Band	Knot	ΔX	ΔY	Relative Strength	FWHM
R	1	+3″.88	−1″.70	475	2″.16
	2	−8.76	−1.74	592	1.83
	3	0.0	0.0	378	2.13
	4	−13.45	0	209	2.19
I	1	+3.73	−1.24	405	2.54
	2	−8.46	−1.74	373	2.0
	3	0.0	0.0	406	2.51
	4	−13.19	0.2	194	2.4
Hα.....	1	+4.65	−2.5	226	2.1
	2	−8.29	−2.24	462	2.1
	3	0.0	0.0	52	2.3
	4	−13.29	+0.74	89	2.9

NOTE.—Relative positions in each band were taken relative to knot 3. The strengths are relative for each band image; positions, relative strengths, and FWHM were taken from the routine splot in IRAF.

2.2. *The Spectra of the Innermost Region*

The sky was carefully selected for two cases. In the first case, only the pixels not affected with any galaxy emission were selected. In the second case, we have eliminated the narrow-line emissions from the galaxy in order to isolate the broad-line components of the western spectrum. We believe that the second case does not affect the possible emission of broad-line components of [S II] and [N II]. If broad [N II] components exist, they are probably blended with the observed broad Hα line, but this is not the case for broad [S II].

Figure 5 shows the spectra from the eastern and western parts of the central regions of NGC 4691 calibrated in wavelength, sky (case II), and flux, but not in redshift. The eastern spectrum shows "normal" narrow Hα, [N II], and [S II] lines. The western spectrum also shows these narrow lines but with an additional broad Hα component. The narrow lines in both eastern and western parts have the redshift of the normal galaxy. The instrumental FWHM, $\mathrm{FWHM}_{\mathrm{instr}} \simeq 3.23$ Å, was obtained from fits to several isolated lines from the comparison lamp spectra. The lines from the NGC 4691 spectra were then fitted and their flux was obtained using the routine splot of IRAF. Table 3 lists the results for the broad and narrow lines.

Redshift determination.—The redshift was derived with the relation $z = (\lambda_{\mathrm{obs}} - \lambda_{\mathrm{rest}})/\lambda_{\mathrm{rest}}$. Using the narrow Hα line, one obtains $z \simeq 0.00372$ for the eastern spectrum. This redshift translates into a systemic recession velocity of $v \simeq 1116 \pm 3$ km s^{-1}, which corresponds to the velocity reported for NGC 4691 from optical (de Vaucouleurs & de Vaucouleurs 1967; Chromey 1974; Sandage 1978), neutral hydrogen (Richter & Huchtmeier 1987), and CO observations (Wiklind et al. 1993). The redshift computed with the [S II] lines is a bit different, $z \simeq 0.00384$, and it corresponds to a systemic velocity of $v \simeq 1150 \pm 3$ km s^{-1}. This velocity difference, about 30 km s^{-1}, could be ascribed to internal gas motions within the galaxy, and we conclude that the spectrum with narrow lines is generated in the disk of the galaxy.

Figure 6 shows the observed eastern and western spectra corrected to the redshift of the galaxy using the sky described as case I. Figure 7 shows the spectra calibrated in redshift, except that the narrow lines were subtracted in an attempt to isolate the broad Hα line (case II for sky). The centroid of the broad Hα line in the western spectrum is blueshifted with respect to the narrow-line component and has a *redshift* of

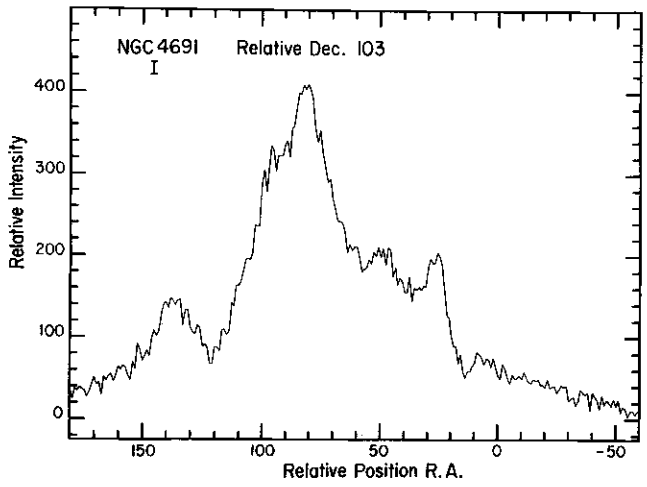

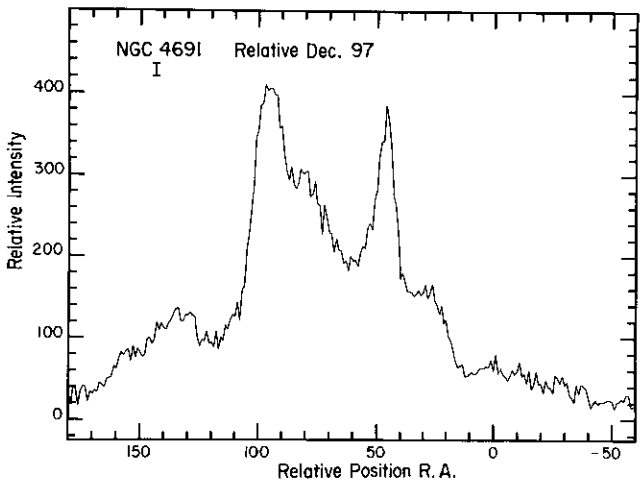

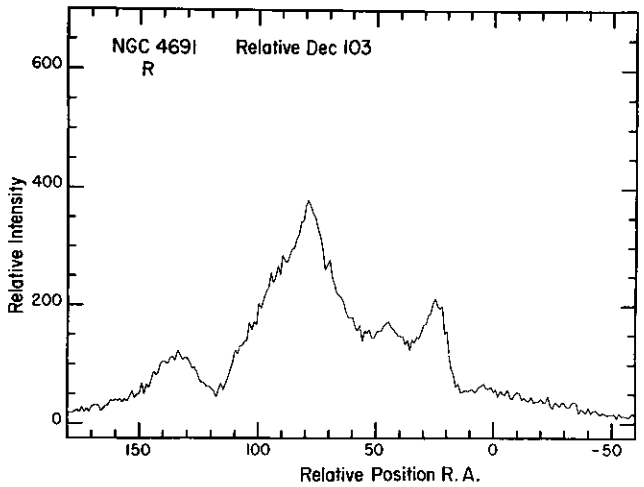

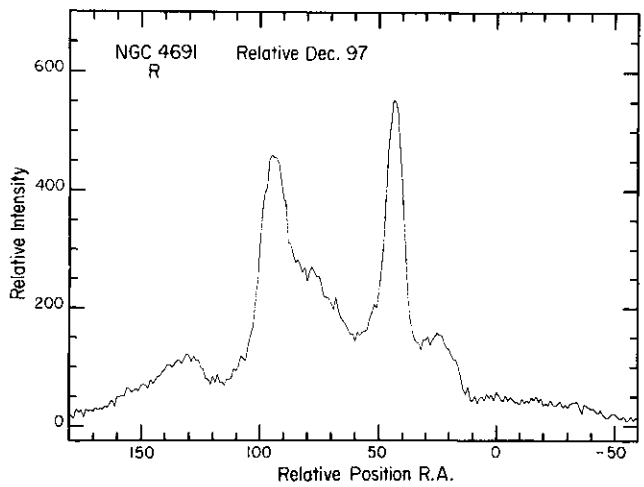

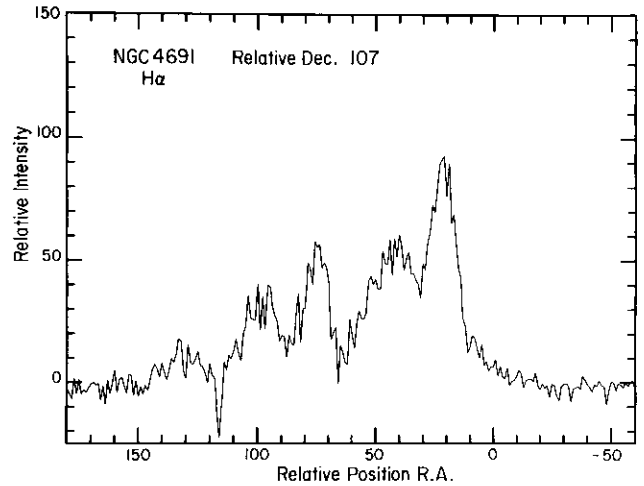

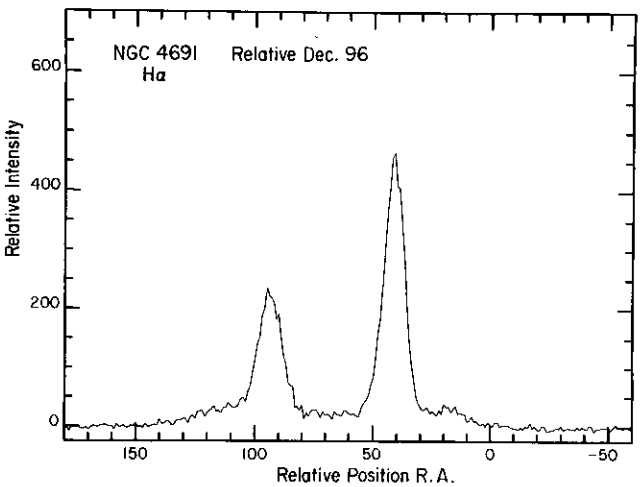

FIG. 4*a*

FIG. 4*b*

FIG. 4.—(*a*) One-dimensional plots of the relative strengths of the *I* (*upper*), *R* (*middle*), and Hα (*bottom*) images at a fixed declination of knots 3 and 4. East is left and west is right. (*b*) same as (*a*), but at a constant declination of knots 1 and 2.

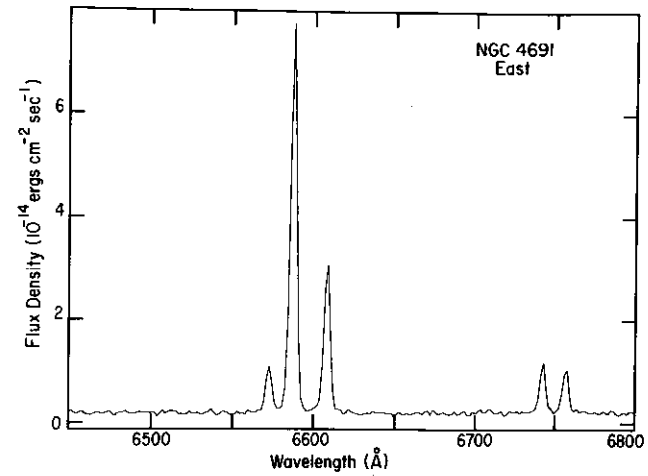

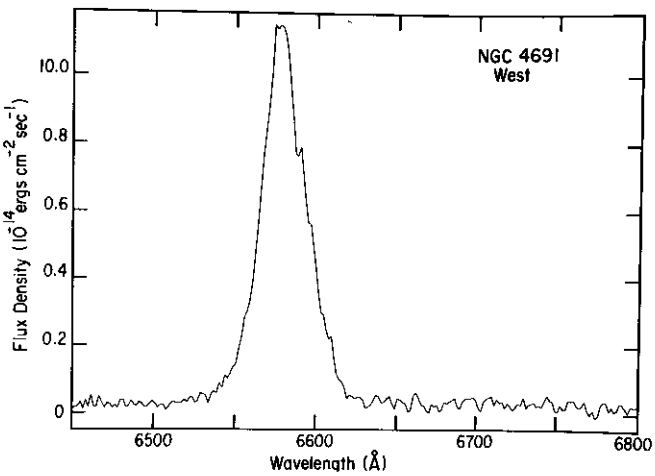

FIG. 5.—Spectra from the eastern (*upper*) and western (*lower*) parts of the barred galaxy NGC 4691 calibrated in wavelength, sky, and flux, but not in redshift. The western spectrum, with a broad Hα line, was obtained after subtraction of the sky assuming that the weak [N II] and [S II] lines, seen in Fig. 3, have the redshift of the normal galaxy.

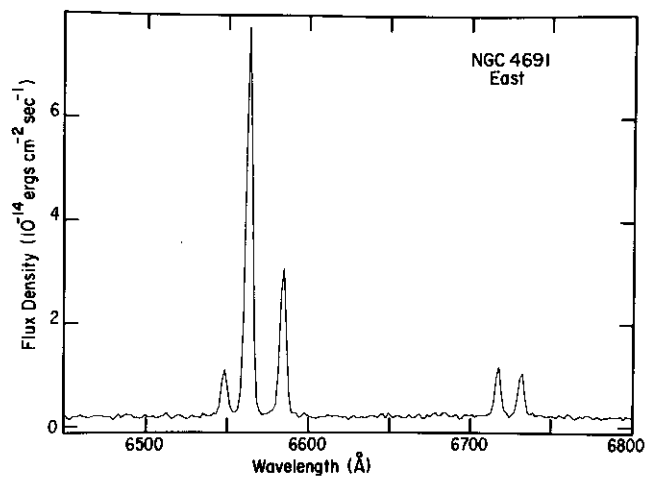

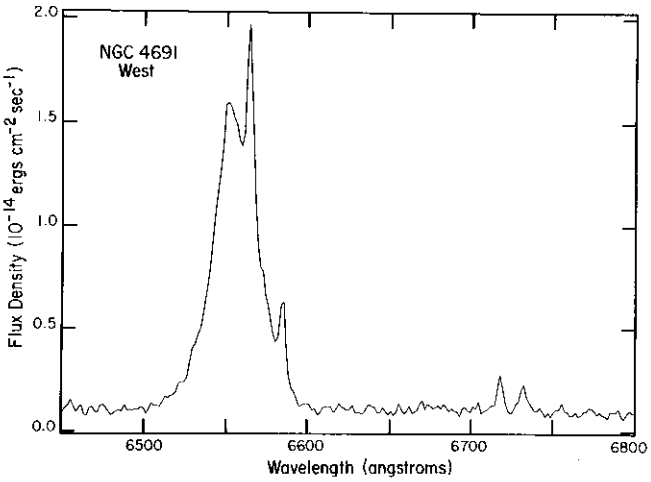

FIG. 6.—Spectra of the innermost region of the barred galaxy NGC 4691 calibrated for the redshift as determined from the Hα line of the upper (eastern) spectrum. The lower (western) spectrum was obtained assuming that the N II and S II lines belong to the object at the redshift of the upper plot and were not subtracted (as part of the sky).

TABLE 3

OPTICAL EMISSION LINES IN THE INNERMOST REGION OF NGC 4691

Line	λ_{rest} (Å)	λ_{obs} (Å)	V[a] (km s^{-1})	FWHM[b] (Å)	FWHM (km s^{-1})	Flux[c]
Narrow Lines						
[N II].....	6548.1	6572.4	1112.5	3.24	148.3	4.5
Hα.....	6562.8	6587.24	1116.4	3.09	141.1	35.4
[N II].....	6583.4	6608.17	1127.9	2.94	133.9	13.9
[S II]	6716.4	6742.25	1153.8	2.60	116.0	4.5
[S II]	6730.8	6756.67	1152.3	3.16	140.7	4.2
Broad Lines						
Hα.....	6562.8	6577.03	650.0	31.0	1207.1[d]	37.2

[a] Velocities computed from $V = (\lambda_{obs} - \lambda_{rest})c/\lambda_{rest}$, where c is the velocity of light (the typical error in the velocity determination is ± 5 km s^{-1}).

[b] FWHM deconvolved with an instrumental response $FWHM_{inst} \simeq 3.23$ Å.

[c] Flux is in units of 10^{-14} ergs s^{-1} cm^{-2}.

[d] Typical error in the velocity width is ± 50 km s^{-1}.

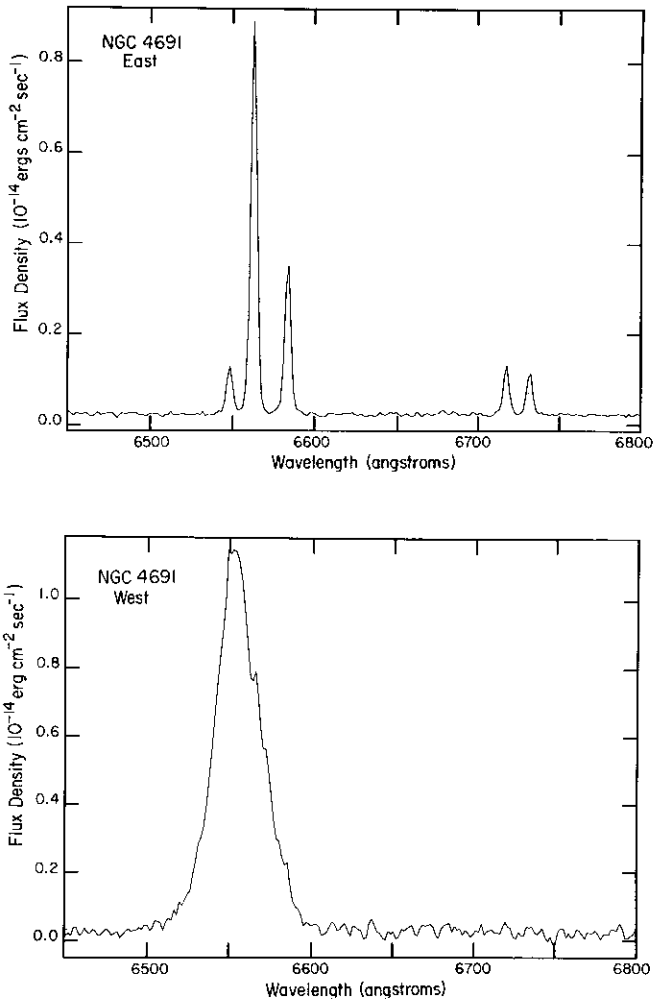

FIG. 7.—Spectra calibrated in redshift except that the western spectrum (*lower*) was obtained after subtracting the narrow-line components (as if they were part of the sky) in an attempt to isolate the broad Hα component.

$z \simeq 0.00217$, corresponding to a systemic velocity of $v \simeq 650$ km s^{-1}. The possible implications of the presence of this broad line and its velocity difference are discussed in the next section.

Line widths.—The FWHM for the [N II], Hα and [S II] lines of the eastern spectrum range from $\Delta V = 116$–148 km s^{-1} and are similar to the H I line width reported by Richter & Huchtmeier (1987), $\Delta V_{\rm H\,I} \simeq 132$ km s^{-1}. The corresponding FWZI for the narrow Hα line is only about $\Delta V \simeq 625$ km s^{-1}, and all these values correspond to those expected in a normal spiral galaxy (Rubin, Whitmore, & Ford 1988).

The FWHM and FWZI for the broad Hα line in the western spectrum, ΔV(FWHM) $\simeq 1207^{+180}_{-5}$ km s^{-1} and ΔV(FWZI) $\simeq 3875 \pm 50$ km s^{-1}, respectively, are certainly large for a normal galaxy and seem to be closer to the characteristic values observed in Seyfert galaxies (Osterbrock 1989; Wilson & Nath 1990).

Is there any blueshifted [N II] *and* [S II]?—Figure 6 shows the spectra of both the eastern and western regions, corrected for the redshift of the galaxy, $z \simeq 0.0037$. As stated before, the western spectrum shows narrow lines superposed on the broad Hα line, and the peak intensity of this broad component is blueshifted with respect to the narrow lines. The intensities of the western [S II] lines are about 10 times weaker than in the eastern spectrum, and there is a small wavelength difference between the [S II] lines in the two spectra of $\Delta\lambda \simeq 1.5$ Å. The corresponding velocity difference in these two sets of lines is about 60 km s^{-1}, which is about twice the redshift difference between the narrow Hα and the [S II] lines and could well be a result of errors in correcting for the system redshift.

More important, however, is the fact that there are no broad or blueshifted [S II] components in the western spectrum at the level of our signal-to-noise ratio (see Fig. 6). The widths of the weak [S II] lines in this western part, on the other hand, are similar to those obtained in the eastern part. Subtracting the narrow lines from the western spectrum, defined as case number two for the sky selection in the previous section, we do not see any trace of [S II] at all (see Figs. 5 and 7). This sets a lower limit on the electron density of the region emitting the broad Hα component. In the case of the [N II] lines of the western spectrum, [N II] λ6584 is clearly superposed on the broad Hα line and is at the redshift of the galaxy. In Figure 7 one notices several small features that, if real, could be identified as weak components of [N II]. One of them, at $\lambda = 6584$ Å, clearly corresponds to a residual of the subtraction of the normal narrow [N II] λ6583.4 line. We should stress that the shoulders at 6580, 6571, and 6565 Å could be spurious features from the subtraction process. However, if real, they could be interpreted as the blueshifted components of [N II] λ6583.4. If this were the case, they indicate blueshifted velocities of 155, 565, and 840 km s^{-1}, respectively. The feature at $\lambda = 6530$ Å, if real, could be interpreted as a blueshifted component of [N II] λ6548.1 with a velocity of 815 km s^{-1}. Obviously, additional high-resolution observations are needed to clarify this issue, but the possible existence of these components sets important constraints on the electron densities of the regions generating the broad components.

Line ratios.—The line ratios in the eastern spectrum are Hα/([N II] λ6583.4) ≃ 2.54, Hα/([N II] λ6548.1) ≃ 7.86, Hα/(N II] λ6548.1 + [N II] λ6583.4) ≃ 1.92, [N II] λ6583.4.1/([N II] λ6548.1) ≃ 3.1, Hα/([S II] λ6716.4 + [S II] λ6730.8) ≃ 4.06, [S II] λ6716.4/[S II] λ6730.8 ≃ 1.07.

Notice that all the [N II]/Hα ratios along with the ratio of [O III]/Hβ (Chromey 1974) give characteristic values of disk H II regions (or even perhaps nuclear H II regions; Kennicutt et al. 1989), and that the [S II] line ratio indicates an electron density of $n_e \simeq 700$ cm^{-3}.

In the case of the western spectrum, the corresponding [N II] line ratios cannot be estimated with reliability because of the broad Hα component. In the case of the [S II] lines, their ratio is similar to that of the eastern part, and the resulting electron density is also similar. Thus, the regions emitting the narrow-line components have electron densities of about 700 cm^{-3}, but the lack of broad [S II] lines implies densities well in excess of 10^4 cm^{-3} for the broad Hα emitting region. If one assumes that the possible [N II] bumps are not real, the lack of broad [N II] lines would imply densities above $\sim 10^5$ cm^{-3} (see Table 3.11 in Osterbrock 1989).

3. DISCUSSION

The overall optical appearance of NGC 4691 indicates a "normal" barred spiral galaxy, but the central regions display symmetrical gas structures and vigorous star-forming activity with evidence for energetic events. Here we discuss a series of different possibilities to understand the spatial structure and the origin of the fast-moving gas.

3.1. *Position of the Compact Nucleus of NGC 4691*

Of particular importance for the discussion of the present data is the position of the compact nucleus. Its exact location *has not* been properly addressed so far. In Table 4 we list the positions associated with the compact central region of NGC 4691 reported by several authors, using different techniques and different wavelengths. Chromey (1974), for example, reports that he carried out his observation around the geometrical center of the galaxy, but gives no coordinates for the position of the central region of NGC 4691. Devereux (1987) reports 10 μm observations with a 5".5 aperture centered on the brightest optical region of NGC 4691 but again gives no coordinates for the compact nucleus. Gallouët, Heidmann, & Dampierre (1975) determined the best optical position of the galaxy from a Palomar Sky Survey film using a Zeiss micrometer machine. For NGC 4691, given the peculiar structure of the central region, we believe that the POSS plate is not the best image to locate the position of the compact nucleus. We note, however, that the position adopted for the optical nucleus by many authors is the position reported by Gallouët et al. (1975). Low-resolution observations at centimeter and millimeter wavelengths can only give the best mean position of the peak intensity of the radio continuum (beam size 1', Condon 1987) and CO emission (beam size 43", Tacconi et al. 1991; beam size 13", Wiklind et al. 1993), but they cannot pinpoint the location of the compact nucleus. Hummel et al. (1987), on the other hand, report high-resolution observations of the radio continuum emission at 1.49 GHz using a beam of only 1".3. Their position of the central radio continuum emission is also given in Table 4. The intensity of this radio continuum component is only 4 mJy and could be interpreted as arising from either a very weak compact nucleus or to a circumnuclear H II region. Similar circumnuclear H II regions have been observed in other normal barred galaxies with no radio continuum emission from the compact nucleus; for example, in NGC 4314 and in NGC 1326 (García-Barreto et al. 1991a, c).

From our set of observations, the location of the compact nucleus seems to be marked by knot 3. Our images show that knot 3 is the strongest feature at the *I* band and the weakest in Hα. It is also located at the geometrical center of the *R* and *I* extended emission images. Since the compact nuclei of other normal barred galaxies are also bright in the *I* band and weak in Hα emission (see, for example, NGC 3351, Kennicutt et al. 1989; NGC 4314, Benedict et al. 1993; NGC 1326, García-Barreto et al. 1991c), we therefore suggest that knot 3 defines the position of the compact nucleus. An optical rotation curve with Fabry-Perot techniques would be extremely useful in order to determine the dynamical center of the galaxy NGC 4691.

3.2. *Possible Origin of the Innermost Spatial Structure*

The spatial structure of the emitting gas in the innermost region of NGC 4691, with four bright knots, is very intriguing. The distribution of the knots is very symmetrical (two similar pairs), and the linear extent of these pairs is also very similar. Carbon monoxide observations by Wiklind et al. (1993) show molecular emission in the bar, and this gas seems to be concentrated in two major complexes symmetrically located around the nucleus in the east-west direction. These bright peaks are separated from each other by about 24", but the authors do not indicate the exact position of the nucleus. A weak CO peak at the midpoint of the main CO peaks, but with a 10" north displacement, was interpreted as originating from an inclined disk or from a molecular gas outflow. Notice, however, that they do report the existence of blueshifted gas with velocity dispersions of only 30–45 km s^{-1}, yet *they do not* report any higher velocity molecular gas (the reasons for this are unclear, but one possibility is that they tuned the receiver only at the expected velocity of the normal galaxy). The separation among the optical knots is only $\simeq$12"; therefore, the ionized gas lies inside the CO peaks. Both the optical and CO peaks are oriented in the same east-west direction. Low-resolution radio continuum emission at 20 cm with a beam size of about 60" (Condon 1987) shows an unresolved source associated with the central regions of NGC 4691 and an additional unresolved source at an angular distance of about 82" to the SE with no bright optical counterpart. The relative orientation between these two sources is similar to the relative orientation between the optical knots 1 and 3 or 2 and 4.

Is NGC 4691 a merger?—The remarkable symmetric structure in the *R*, *I*, and Hα images (Figs. 1 and 2) could be interpreted as resulting from a merger. The *IRAS* fluxes at the

TABLE 4

POSITIONS OF THE CENTRAL REGION OF NGC 4691

R.A.(1950.0)	Decl.(1950.0)	Method	Reference
12^h45^m6	−03°04′	Optical	de Vaucouleurs & de Vaucouleurs 1967
	...	Optical	Chromey 1974[a]
$12^h45^m39^s.5 \pm 0.4$.....	−03°03′28" ± 3	POSS	Gallouët et al. 1975
$12^h45^m39^s$	−03°03′.6	Optical	Sandage 1978
12^h45^m6	−03°04′	Hα	Keel 1983
$12^h45^m38^s.9$.....	−03°03′39"	Radio continuum	Condon 1987[b]
	...	IR 10 μm	Devereux 1987[c]
$12^h45^m39^s.5$.....	−03°03′28"	H I	Richter & Huchtmeier 1987[d]
$12^h45^m39^s.38$	−03°03′39".3	Radio continuum	Hummel et al. 1987[e]
$12^h45^m40^s$	−03°03′30"	CO	Tacconi et al. 1991[f]
$12^h45^m38^s.7$.....	−03°03′36"	CO	Wiklind et al. 1993[g]

[a] Geometric center.
[b] Beam size $\simeq$ 1'.
[c] Centered on the brightest optical object (5".5 aperture).
[d] H I beam 10'.
[e] Beam size $\simeq$ 1".3.
[f] CO(1–0) beam 43".
[g] CO(2–1) beam 13".

far-infrared wavelengths indicate (1) a high FIR luminosity, $L_{FIR} \simeq 10^{10}\ L_\odot$, (2) a relatively high dust temperature, $T_d \simeq 40$ K, and (3) *IRAS* colors characteristic of a galaxy having undergone recent star formation (see, e.g., Helou 1986).

As mentioned before, the dust temperature is similar to those derived in strongly interacting galaxies, $\langle T_{inter} \rangle \simeq 41$ K (type 4 of Solomon & Sage 1988), whereas the *IRAS* FIR and CO luminosities are more similar to those of weakly interacting galaxies (type 0 or 1 of Solomon & Sage 1988). Also, among 35 barred galaxies with $\langle T_{av} \rangle \simeq 30$ K and $\langle L_{av} \rangle \simeq 5.6 \times 10^9\ L_\odot$ (García-Barreto et al. 1991a, b, c, 1993), NGC 4691 has the second highest dust temperature as well as a high FIR luminosity. The Palomar image shows NGC 4691 as an almost face-on barred galaxy with two long spiral arms extending in the N-S direction, but there is no evidence for tidal tails or for any other feature that could be ascribed to a recent interaction. The closest galaxy on the plane of the sky, NGC 4684 with $v_{sys} \simeq 1589$ km s^{-1}, is located some 11 galaxy diameters away in the NW direction. The velocity difference rules out any physical association and, at best, one could say that NGC 4691 is a weakly interacting galaxy of type 0 (Solomon & Sage 1988).

Are the structures a result of gravitational lensing?—The peculiar symmetry of the structures could be interpreted as resulting from gravitational lensing from a massive foreground object. The right ascension separation of the two bright knots is similar to the distance between the two weaker knots. Similarly, the two eastern knots are separated in declination a similar distance as the two western objects. The large angular separation, however, rules out the gravitational lensing interpretation. The nature of the alignment is unknown, but it seems to be a coincidence, since there are additional structures that could be interpreted as the starting point of the spiral arms in the most southeasterly and northwesterly parts of the images. The knots could very well just be giant molecular clouds with embedded giant H II regions moving in the deepest part of the gravitational potential well.

Are the structures a result of galactic dynamics?—In spiral galaxies, the orbits of the stars and the gas can crowd at specific distances from the galactic center, forming the so-called Lindblad Resonances. In particular, the gas is transferred inward from the corotation radius to the Inner Lindblad Resonance (ILR) in orbits parallel to the bar. Inside the ILR, the gas rotates in orbits perpendicular to the orientation of the bar (Binney & Tremaine 1987). The structure seen in our optical images could be interpreted as if the four bright optical knots were part of a nuclear ring inclined to our line of sight. This would explain the highly symmetrical distribution, but it would require the compact nucleus to be at the midpoint. In NGC 4691 there is no bright central source in either the *I*, the *R*, or the Hα images, but this could very well be because it is outshined by the bright knots.

3.3. *Possible Nature of the Broad-Line Spectrum*

The spectroscopic observations of de Vaucouleurs & de Vaucouleurs (1967), Chromey (1974), and Sandage (1978) indicate that they studied only the *eastern* spectrum of the galaxy. It is unclear if they simply missed the second spectrum or if the broad component was very faint, or did not exist at all, at that time. Some facts, however, seem to indicate that the broad components were problably faint or nonexistent. Chromey used a long slit, with 30″, at several different position angles. Three of them were along the bar (P.A. $\simeq$ 240°, 260°, and 270°), and he should have noticed the broad-line spectrum on the western side of the galaxy if it existed at the same time. Similarly, using the 5 m Palomar telescope, Sandage reports the existence of extended emission across the decker at P.A. $\simeq$ 79 for the NGC 4691 observations, and he reports that the overall conditions of the measurements were excellent. It is difficult to imagine that he missed the broad component under these conditions.

There is a series of separate possibilities for the nature of the broad Hα component. The spectroscopic analysis of the eastern spectrum indicates that it is associated with a normal H II region nucleus galaxy, with a systemic velocity of $V \simeq 1116$ km s^{-1} at a distance of about 22.3 Mpc, in agreement with other optical and radio observations. We therefore assume that NGC 4691 is at that distance and discuss briefly some possibilities for the origin of the broad component under this assumption.

Is NGC 4691 a Seyfert galaxy?—A broad Hα line width of a few thousand km s^{-1} could be associated with the nuclear activity of a Seyfert galaxy. The western spectrum of NGC 4691 displays a large velocity, $\Delta V_{FWHM} \simeq 1200$ km s^{-1}, characteristic of a Seyfert 2 galaxy (Osterbrock 1989). The physical conditions indicated by the observed line ratios for the eastern spectrum, in addition to the line ratios of oxygen and Hβ derived by Chromey (1974), suggest a normal H II region nucleus (see also Kennicutt et al. 1989). There are several galaxies which display composite properties of both starburst and Seyfert nuclei (e.g., Marziani et al. 1994), and the far-infrared properties of Seyfert 2 galaxies indicate strong star formation activity (e.g., Dultzin-Hacyan & Benitez 1994). Thus, NGC 4691 could well be a galaxy with a composite nuclear region. Two arguments against this Seyfert-like interpretation, however, are that the centroid of the broad Hα line is blueshifted with respect to the galaxy ($z_{east} \simeq 0.00372$ and $z_{west} \simeq 0.00217$) and that the western broad-line knot is *not* coincident with the compact nucleus (§ 3). The active region would then be displaced from the compact nucleus and moving away from the galaxy, extremely unusual and unlikely properties for these types of objects. As a result of the distance of NGC 4691 and the fact that there is no optical evidence of any foreground object on either the Palomar plates or any other more recent optical photograph of the galaxy (see Sandage 1962 and our Fig. 1), we believe that the possibility of the existence of a foreground galaxy is extremely unlikely.

Is the broad-line component a result of an expanding shell or a galactic wind?—The narrow [N II] and [S II] lines of the western spectrum are at the redshift of the galaxy, and the centroid of the broad Hα component is blueshifted by some 500 km s^{-1} with respect to these lines (see Fig. 6). One could therefore conclude that the narrow lines are produced in H II regions located within the gaseous disk, whereas the broad Hα line arises from an ionized gaseous component that is outflowing from the disk. This outflow could be ascribed to an expanding supernova-driven shell or to a galactic wind that is almost aligned with our line of sight. We favor the scenario of having an expanding shell due to supernovae because of the lack of broad [S II] lines.

In this interpretation, one might expect a shell of atomic hydrogen also to be ejected. The H I spectrum presented by Richter & Huchtmeier (1987) shows the main line at the velocity of the galaxy, $V \simeq 1115$ km s^{-1}, *plus* weak emission at $V \simeq 600$ km s^{-1} very similar to the centroid of the broad component. Obviously, Richter & Huchtmeier disregarded any

association with the weak emission because it was not expected. New observations of H I and CO with higher spatial resolution and covering a wider bandwidth would be desirable. Also, given that no OH megamasers have been found at the velocity of the normal galaxy (Baan, Haschick, & Henkel 1992), a new search with an extended bandwidth would be desirable.

To conclude, a fast-moving or expanding shell is the most likely origin of the broad component, and we focus on the details of this idea in the following section.

4. EXPANDING SHELLS AND GALACTIC WINDS

Expanding shells are commonly detected as optical or 21 cm line structures, surrounding either single massive stars or OB associations in our Galaxy and other nearby gaseous galaxies (e.g., Chu, Treffers, & Kwiter 1983; Tenorio-Tagle & Bodenheimer 1988; Dufour 1989; Dubner, Niemela, & Purton 1990; Brinks 1994; Rosado, Le Coarer, & Georgelin 1994). Evidence for the presence of galactic winds, on the other hand, has been reported in several galaxies (e.g., Ford et al. 1986; Armus, Heckman, & Miley 1990; Duric & Seaquist 1988; Heckman, Armus, & Miley 1990; Filippenko & Sargent 1992; Dettmar & Leiber 1993). Both expanding shells and galactic winds are a result of the same type of perturbation: mechanical energy injection from massive stars.

The basic event is the bubble created by the action of a single star: a wind-driven cavity, or the composed remnant created by a supernova exploding in a wind-driven cavity. The sizes and properties of these structures depend on both the stellar energy input and the density of the ambient medium (e.g., Tenorio-Tagle et al. 1990, 1991; Terlevich et al. 1992; see review by Franco 1994). The combined effect of stellar winds and supernovae from a stellar cluster can drive large superbubbles and, if the expanding structure is able to break out of the disk, can pump mass and energy into the galactic halo (e.g., Bruhweiler et al. 1980; Mac Low, McCray, & Norman 1989; Norman & Ikeuchi 1989; Heiles 1990; Silich et al. 1994; see reviews by Tenorio-Tagle & Bodenheimer 1988 and Tomisaka 1994). If the thermal velocity of the halo gas remains below the escape velocity, the gas simply circulates in a galactic fountain (e.g., Shapiro & Field 1976; Chevalier & Oegerle 1979; Ferrara & Einaudi 1992). When the energy injection rate into the halo reaches a certain critical value, the outflow can overcome the gravitational potential of the host galaxy and a galactic wind is created (e.g., Chevalier & Oegerle 1979; Tomisaka & Ikeuchi 1988; Heckman et al. 1990; see review by Habe 1994). Thus, the energy injection provides an appropriate feedback control to the mass exchange among the disk and the halo and, depending on the star formation rate, the expanding shells can create fountains or winds at galactic scales.

The expansion velocity inferred from the observed broad Hα component, some 500 km s^{-1}, is within the expected velocity range for a galactic wind (e.g., Heckman et al. 1990). The existence of Hα emission, in turn, indicates that a cooling shell has already formed and that the outflow should be in an advanced evolutionary stage (e.g., Habe 1994). The size of the expanding region, however, restricts the validity of this interpretation. The extent of the bright western knot (knot 2 in Fig. 2) provides an upper limit to the diameter of the expanding *shell*. As stated before, its FWHM angular size of 2".13 corresponds to a linear diameter of about 240 pc. This is very small for a mature galactic outflow unless, of course, the outflow is highly collimated or is still in an early stage. The possibility of a highly collimated outflow cannot be completely ruled out by the present observations, but unless there is a strong *B*-field tube almost aligned along our line of sight, it seems very unlikely.

The presence of an Hα shell during the early stages of galactic wind evolution, on the other hand, would indicate that this is not really a wind, but either a single supernova remnant evolving inside an H II region or a multisupernova shell (a superbubble) carving its way out into the halo.

Supernovae interacting with normal H II regions display broad Hα and [S II] line components (Rosado et al. 1994). In fact, shocked regions in general have very strong [S II] emission, and the broad-line components of either resolved or unresolved sources are more easily detected in sulfur emission than in Hα. Thus, both normal SN remnants evolving inside H II regions or superbubbles emitting in Hα should display very strong [S II] emission. As already stated, the fact that the broad [S II] component is not present indicates that the expanding shell has densities well in excess of $n_e \sim 10^4$ cm^{-3} (see Table 3.11 and Fig. 5.3 in Osterbrock 1989). A conservative estimate indicates that the missing broad-line components are at least an order of magnitude fainter than the detected narrow lines, and the expanding shell should have densities above some 10^5 or 10^6 cm^{-3}.

Such a large density, along with the large speed, indicates that the expanding shell is probably a "compact supernova remnant" generated by one or several exploding massive stars that were still embedded in their parental molecular cloud or H II region (Terlevich et al. 1992, 1995; Franco, Arthur, & Miller 1994). Actual evidence for SN remnants with broad optical emission lines, resembling Seyfert galaxies, has been reported by Filippenko (1989), and the origin of the broad Hα component could well be ascribed to this new type of object. For SN remnants evolving in ambient densities below 10^5 cm^{-3}, the transition from a nearly adiabatic to a strongly radiative shock occurs at about the time of thin shell formation, t_{sf}. A large fraction of the SN energy is radiated away by this process, and the remnant reaches its peak luminosity during this epoch. The onset of thin shell formation occurs at the time (Franco et al. 1994b)

$$t_{sf} \simeq 2.87 \times 10^4 E_{51}^{3/14} n_0^{-4/7} \text{ yr} . \quad (1)$$

where E_{51} is the energy in units of 10^{51} ergs, and n_0 is the number gas density in the ambient medium. The maximum luminosity is achieved at about $1.65t_{sf}$, and the strongly radiative epoch is over at about $1.8t_{sf}$. Thus, the gas is compressed into a thin and cool shell in a timescale of about $0.8t_{sf}$. The average remnant luminosity during this epoch of strong radiative cooling can be approximated by

$$\langle L \rangle \sim 1.2 \times 10^5 E_{51}^{11/14} n_0^{4/7} L_\odot , \quad (2)$$

and the maximum luminosity is, roughly, a factor of 2 above this value. The average radiative flux coming out from the remnant during shell formation scales as $E_0^{3/14} n_0^{10/7}$, and the average temperature of the emitting gas scales as $E_0^{2/14} n_0^{2/7}$ (Franco et al. 1994a). All these dependences show that the timescales for cooling become shorter but the emitted spectra became harder and the photoionizing flux increases as the ambient density increases. Thus, remnants evolving in high-density media generate a large ionizing flux and create bright photoionized regions ahead of the shock front. At densities of the order of 10^5 cm^{-3} the onset of thin shell formation occurs only some 40 yr after ejecta thermalization, and the average

luminosity of a single remnant reaches values of about 8×10^7 $L_\odot$, which are similar to the luminosities of an entire massive cluster. This formulation is not valid above $n_0 \sim 10^5$ cm^{-3} because the strong cooling regime occurs before ejecta thermalization is completed, and only a reduced fraction of the SN energy participates in the strong cooling regime. Nonetheless, detailed numerical models of remnants evolving in ambient densities of 10^7 cm^{-3} indicate that these objects can reach Hα luminosities of about 10^6 $L_\odot$ in timescales of less than 10 yr after the explosion (Terlevich et al. 1992, 1995; Franco et al. 1993). Together these results show that SN remnants in ambient densities above 10^4 cm^{-3} can reach peak luminosities between 10^6 and 10^8 $L_\odot$, and they should have an obvious impact in regions with vigorous star formation: they should create bright photoionized regions, as bright as an entire massive stellar cluster, with peculiar large-velocity features. This scenario can explain the outflow in NGC 4691 and, given the short timescales for thin shell formation, could also explain the reason why the broad Hα component was missed in previous studies: *it probably was not there.*

The observed luminosities are in agreement with those expected from a compact SN remnant embedded in a large H II region. The Hα luminosity of the narrow-line spectrum is $L_{H\alpha} \simeq 2 \times 10^{40}$ ergs s^{-1}, in agreement with the luminosity derived by Keel (1983). If all this emission is generated in "normal" H II regions, then the suggested number of Lyman continuum photons, $\sim 3 \times 10^{51}$ s^{-1}, is equivalent to about 5000 O7 stars (see Panagia 1973). This is consistent with the IR results reported by Puxley et al. (1990), which require some 10^{52} s^{-1} ionizing photons to excite the entire central IR emission. The extent of the bright western knot seen in Figure 2 could be interpreted as a characteristic diameter of a giant molecular cloud, with H II regions embedded, at the disk of the galaxy. The Hα luminosity of the broad-line component is also similar, $L_{H\alpha} \simeq 2 \times 10^{40}$ ergs s^{-1}, indicating a similar energy output in both the emission from the quiet and fast ionized gas. Thus, the Hα luminosities indicate that all knots have an important contribution from normal H II regions and that the broad-line component is only an additional component, probably excited by a compact SN remnant.

5. CONCLUSIONS

We have presented new broadband and narrow-band imaging and spectroscopic observations of the central region of the barred spiral galaxy NGC 4691. A broad Hα line has been detected with a velocity centroid at a bluer velocity relative to the normal galaxy. Our observations are interpreted as having a normal galaxy at a distance of about 22 Mpc with an expanding shell. This perturbed gas could be driven by the action of one or various compact supernova remnants evolving in the H II regions located close to the center of the galaxy. The possible existence of [N II] at bluer velocities than the systemic velocity of the galaxy and the lack of any blue velocity component of [S II] suggest that the ambient electron density is high and that [S II] is probably collisionally de-excited. More spectroscopic observations are needed in order to confirm the existence of the [N II] lines at bluer velocities, Likewise, more dynamical studies are needed in order to determine the position of the compact nucleus.

We would like to thank Gloria Koenigsberger and Margarita Rosado for useful discussions on massive stars and the observed properties of SN remnants embedded in H II regions, and Warren Miller for a critical reading of the manuscript. J. F. acknowledges partial support from DGAPA-UNAM through the grant IN105894 and from CONACYT through the grant 400354-5-484E. J. A. G.-B. acknowledges partial financial support from CONACYT (Mexico) grant 689-E9111. We would also like to thank an anonymous referree for valuable comments and suggestions.

REFERENCES

Armus, L., Heckman, T. M., & Miley, G. K. 1990, ApJ, 364, 471
Baan, W. A., Haschick, A. D., & Henkel, C. 1992, AJ, 103, 728
Benedict, G. F., et al. 1993, AJ, 105, 1369
Binney, J., & Tremaine, S. 1987, Galactic Dynamics (Princeton: Princeton Univ. Press)
Bland, J., & Tully, R. B. 1988, Nature, 334, 43
Brinks, E. 1994, in Violent Star Formation: from 30 Dor to QSOs, ed. G. Tenorio-Tagle (Cambridge: Cambridge Univ. Press), 145
Bruhweiler, F. C., Gull, T. R., Kafatos, M., & Sofia, S. 1980, ApJ, 238, L27
Chevalier, R. A., & Oegerle, W. 1979, ApJ, 227, 39
Chromey, F. R. 1974, A&A, 37, 7
Chu, Y.-H., Treffers, R. R., & Kwitter, K. B. 1983, ApJS, 53, 937
Condon, J. J. 1987, ApJS, 65, 485
Dettmar, R-J., & Lieber, T. 1993 in Star Formation, Galaxies and the Interstellar Medium, ed. J. Franco, F. Ferrini, & G. Tenorio-Tagle (Cambridge: Cambridge Univ. Press), 201
de Vaucouleurs, A., & de Vaucouleurs, G. 1967, AJ, 72, 730
Devereux, N. 1987, ApJ, 323, 91
Dubner, G. M., Niemela, V. S., & Purton, C. 1990, AJ, 99, 857
Dufour, R. J. 1989, Rev. Mexicana Astron. Astrofis., 18, 87
Dultzin-Hacyan, D., & Benitez, E. 1994, A&A, 291, 720
Duric, N., & Seaquist, E. R. 1988, ApJ, 326, 574
Ferrara, A., & Einaudi, G. 1992, ApJ, 395, 475
Filippenko, A. V.1989, AJ, 97, 726
Filippenko, A. V., & Sargent, W. W. 1992, AJ, 103, 28
Ford, H. C., Dahari, O., Jacoby, G. H., Crane, P. C., & Ciardullo, R. 1986, ApJ, 311, L7
Franco, J. 1994, Rev. Mexicana Astron. Astrofis., 29, 91
Franco, J., Arthur, S. J., & Miller, W. 1994a, in Violent Star Formation; from 30 Dor to QSOs, ed. G. Tenorio-Tagle (Cambridge: Cambridge Univ. Press), 387
Franco, J., Miller, W., Arthur, S. J., Tenorio-Tagle, G., & Terlevich, R. 1994b, ApJ, 435, 805
Franco, J., Miller, W., Cox, D., Terlevich, R., & Tenorio-Tagle, G. 1993, Rev. Mexicana Astron. Astrofis., 27, 133
Gallouët, L., Heidmann, N., & Dampiere, F. 1975, A&AS, 19, 1
García-Barreto, J. A., Carrillo, R., Klein, U., & Dahlem, M. 1993, Rev. Mexicana Astron. Astrofis., 25, 31
García-Barreto, J. A., Dettmar, R.-J., Combes, F., Gerin, M., & Koribalski, B. 1991c, Rev. Mexicana Astron. Astrofis., 22, 197
Garcia-Barreto, J. A., Downes, D., Combes, F., Carrasco, L., Gerin, M., & Cruz-Gonzalez, I. 1991b, A&A, 252, 19
Garcia-Barreto, J. A., Downes, D., Combes, F., Gerin, M., Magri, C., Carrasco, L., & Cruz-Gonzalez, I. 1991a, A&A, 244, 257
Habe, A. 1994, in Numerical Simulations in Astrophysics, ed. J. Franco et al. (Cambridge: Cambridge Univ. Press), 151
Heckman, T. M., Armus, L., & Miley, G. K. 1987, AJ, 93, 276
———. 1990, ApJS, 74, 833
Heiles, C. 1990, ApJ, 354, 483
Helou, G. 1986, ApJ, 311, L33
Hummel, E., van der Hulst, J. M., Keel, W. C., & Kennicutt, R. C. 1987, A&AS, 70, 517
Keel, W. 1983, ApJS, 52, 229
Kennicutt, R. C., Keel, W. C., & Blaha, C. A. 1989, AJ, 97, 1022
Mac Low, M.-M., McGray, R., & Norman, M. L. 1989, ApJ, 337, 141
Marziani, P., Keel, W., Dultzin-Hacyan, D., & Sulentic, J. W. 1994, ApJ, 435, 668
Norman, C., & Ikeuchi, S. 1989, ApJ, 345, 372
Osterbrock, D. E. 1989, Astrophysics of Gaseous Nebulae and Active Galactic Nuclei (Mill Valley, CA: Univ. Science Books)
Panagia, N. 1973, AJ, 78, 929
Puxley, P. J., Hawarden, T. G., & Mountain, C. M. 1990, ApJ, 364, 77
Richter, O-G., & Huchtmeier, W. K. 1987, A&AS, 68, 427
Rosado, M., Le Coarer, E., & Georgelin, Y. P. 1994, A&A, 286, 231
Rubin, V. C., Whitmore, B. C., & Ford, K. W., Jr. 1988, ApJ, 333, 522
Sandage, A. 1962, The Hubble Atlas of Galaxies (Washington, DC: Carnegie Institution of Washington)
———. 1978, AJ, 83, 904
Sandage, A., & Tammann, G. A. 1987, A Revised Shapley-Ames Catalog of Bright Galaxies (Washington, DC: Carnegie Institution of Washington)

Shapiro, P., & Field, G. 1976, ApJ, 205, 762
Silich, S., Franco, J., Palous, J., & Tenorio-Tagle, G. 1994, in Numerical Simulations in Astrophysics, ed. J. Franco et al. (Cambridge: Cambridge Univ. Press), 193
Solomon, P. M., & Sage, L. J. 1988, ApJ, 334, 613
Tacconi, L. J., Tacconi-Garman, L. E., Thorney, M., & Woerden, H. 1991, A&A, 252, 541
Tenorio-Tagle, G., & Bodenheimer, P. 1988, ARA&A, 26, 145
Tenorio-Tagle, G., Bodenheimer, P., Franco, J., & Rozyczka, M. 1990, MNRAS, 244, 563
Tenorio-Tagle, G., Rozyczka, M., Franco, J., & Bodenheimer, P. 1991, MNRAS, 251, 318
Terlevich, R., Tenorio-Tagle, G., Franco, J., & Melnick, J. 1992, MNRAS, 255, 713
Terlevich, R., Tenorio-Tagle, G., Franco, J., & Rozyczka, M. 1995, MNRAS, 272, 198
Tomisaka, K. 1994, in Numerical Simulations in Astrophysics, ed. J. Franco et al. (Cambridge: Cambridge Univ. Press), 184
Tomisaka, K., & Ikeuchi, S. 1988, ApJ, 330, 695
Tully, R. B. 1988, Nearby Galaxies Catalog (Cambridge: Cambridge Univ. Press)
Ulrich, M.-H. 1978, ApJ, 219, 424
Whiteoak, J. B., & Gardner, F. F. 1979, Proc. Astr. Soc. Australia, 3, 319
Wiklind, T., Henkel, C., & Sage, L. J. 1993, A&A, 271, 71
Wilson, A. S., & Nath, B. 1990, ApJS, 74, 731

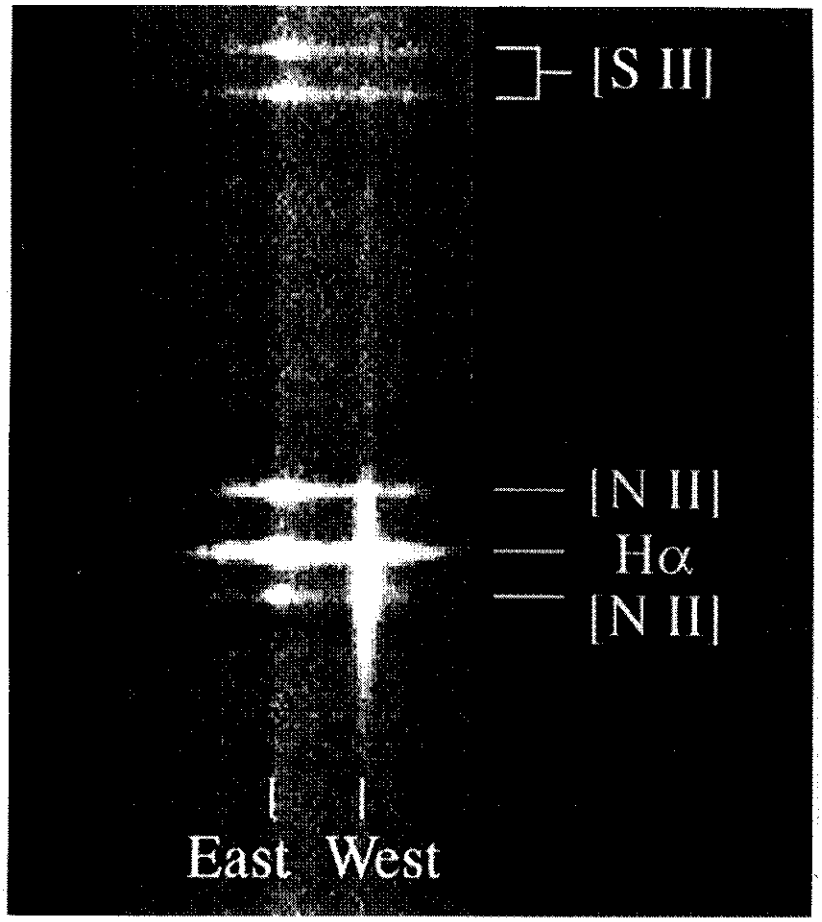

FIG. 3.—Gray-scale image of the spectra observed toward the galaxy NGC 4691. The slit was oriented in the E-W direction at the approximate declination of the two brightest knots seen in Fig. 1*a*. The spectrum seen on the left side (east) corresponds to the bright knot labeled 1, while the spectrum seen on the right side (west) corresponds to the bright knot labeled 2 in Fig. 1*a*.